



This is the accepted manuscript made available via CHORUS. The article has been published as:

## Molecular-field-coefficient modeling of temperature-dependent ferrimagnetism in a complex oxide

Miela J. Gross, Tingyu Su, Jackson J. Bauer, and Caroline A. Ross

Phys. Rev. Applied **21**, 014060 — Published 30 January 2024

DOI: [10.1103/PhysRevApplied.21.014060](https://doi.org/10.1103/PhysRevApplied.21.014060)

# Molecular Field Coefficient Modeling of Temperature-Dependent Ferrimagnetism in a Complex Oxide

Miela J. Gross<sup>1</sup>, Tingyu Su<sup>2</sup>, Jackson J. Bauer<sup>3</sup>, Caroline A. Ross<sup>3\*</sup>

<sup>1</sup>*Department of Electrical Engineering and Computer Science, Massachusetts Institute of Technology, Cambridge, Massachusetts 02139, USA*

<sup>2</sup>*Department of Mechanical Engineering, Massachusetts Institute of Technology, Cambridge, Massachusetts 02139, USA*

<sup>3</sup>*Department of Materials Science and Engineering, Massachusetts Institute of Technology, Cambridge, Massachusetts 02139, USA*

\*To whom correspondence should be addressed. E-mail: [caross@mit.edu](mailto:caross@mit.edu)

The temperature-dependent magnetic moment of a magnetically ordered material is fundamental to all aspects of its technological applications. In ferrimagnetic materials with multiple sublattices containing different magnetic ions, the magnetization can vary nonmonotonically with temperature. Computational modeling of these materials provides insight into their sublattice occupancy and prediction of their behavior as a function of composition. Here we develop a python computer code called DIONNE that models the magnetism of rare-earth iron garnets ( $\text{RE}_3\text{Fe}_5\text{O}_{12}$ , REIG) using molecular field coefficient (MFC) theory. The program calculates the exchange interactions and the magnetic moment of each sublattice to determine the net magnetization and angular momentum as a function of temperature. DIONNE accounts for site occupancy on each sublattice including the effects of non-magnetic and magnetic substitutions, vacancies,  $\text{Fe}^{2+}$ , and deviations from the ideal RE:Fe stoichiometry by considering their effects on the magnetization and exchange coupling. Unlike previous iterative methods, DIONNE recursively solves for the moment at each temperature, yielding an excellent match to magnetization vs. temperature data for a range of bulk garnets. This work predicts magnetic properties of REIGs with a variety of compositions and point defect levels and enables design of ferrimagnets with useful properties.

## Introduction

Ferrimagnetic materials consist of two or more magnetic sublattices with antiparallel coupling, leading to behavior that differs qualitatively from that of ferromagnets. For example, ferrimagnets may show magnetization and angular momentum compensation temperatures, dynamics that resemble those of antiferromagnets, and sublattice-specific optical or electronic properties [1,2]. Ferrimagnets have been used in a range of data storage, logic, photonic, signal processing and sensor devices taking advantage of their spintronic, magneto-optical and microwave properties [1–6]. Ferrimagnetic oxides, particularly yttrium iron garnet, exhibit low Gilbert damping [7–10] and high resistivity [11–13]. Furthermore, thin films of iron garnets can be grown with perpendicular magnetic anisotropy (PMA) which is desirable for many spintronic device applications [14–16]. Predicting and explaining the temperature-dependent magnetization is essential in optimizing garnets and other ferrimagnets for specific applications.

The molecular field theory of Néel [17] has been used successfully to model ferrimagnetic materials [18–20]. The magnetization is separated into contributions from the magnetic species on each sublattice, whose temperature-dependence is represented by Brillouin functions. This, combined with the appropriate molecular field coefficients to model the intra- and inter-sublattice exchange coupling strength, yields the net magnetic moment as a function of temperature. Dionne [19,21–25] applied this theory to yttrium iron garnet and rare earth iron garnets (REIGs,  $\text{RE}_3\text{Fe}_5\text{O}_{12}$ ) and obtained a good quantitative fit to experimental data of magnetization vs. temperature,  $M(T)$  [26–35]. This model addressed a full range of RE substituents as well as limited ranges of nonmagnetic substitutions for Fe. It does not account generally for non-ideal site occupancies such as RE or Fe antisite defects. Modeling the effects of

such defects is particularly important for understanding thin film ferrimagnet properties because epitaxial growth can stabilize films with compositions far from those of bulk crystals [36].

Here we develop a computer program in python, named DIONNE after our colleague Dr. Gerald F. Dionne [37], which models the magnetic moment and angular momentum of REIGs as a function of temperature. The program accounts for a wide range of site occupancies in REIGs, including non-magnetic and magnetic substitutions, vacancies in all sublattices,  $\text{Fe}^{2+}$  substitutions, and deviations from the ideal  $\text{RE}:\text{Fe} = 3:5$  stoichiometry. While prior models calculate the moment iteratively [25,38], DIONNE recursively solves for the moment and angular momentum which increases the accuracy of the model up to the Curie temperature. We validate the model by comparison with data from bulk stoichiometric REIGs as well as those with mixed RE elements and nonmagnetic substitutions. We then model REIGs with large deviations from bulk stoichiometry, in particular Tb-rich TbIG, which enables determination of sublattice occupancy. While DIONNE is used here for REIGs, the approach can be adapted to model  $M(T)$  for other multi-sublattice ferrimagnetic oxides such as spinels [39,40].

### **Description of Model**

REIGs comprise three cation sublattices: tetrahedral  $\text{Fe}^{3+}$  (d-sites), octahedral  $\text{Fe}^{3+}$  (a-sites), and dodecahedral  $\text{RE}^{3+}$  (c-sites), in the ratio of 3:2:3 sites per formula unit of  $\text{RE}_3\text{Fe}_5\text{O}_{12}$ . The strongest coupling is antiferromagnetic superexchange between the Fe in the a- and d-sites, and the c-sites are also coupled antiferromagnetically to the d-site sublattice. Thus, the magnetic

moment  $M$  of the REIG is the absolute value of the d-site moment minus the a-site and c-site moments:

$$M = |M_d - M_a - M_c| \quad (1)$$

where  $M_d$ ,  $M_a$ , and  $M_c$  are the moments of the d-, a-, and c-site sublattices respectively. Following Dionne [19,21–25], we utilize the molecular field theory of Néel [17], which combines the use of molecular field coefficients and Brillouin functions to model the magnetic behavior. Each sublattice moment is the product of the zero-temperature moment, controlling the amplitude, and a Brillouin function, giving the moment as a function of temperature according to the  $S$ ,  $L$ ,  $J$  quantum numbers of the ions occupying the sublattice and the exchange field due to neighboring ions. At a given temperature,  $T$ , the moment of sublattice  $M_{i,T}$  (where  $i$  represents the a, d, or c-site) is expressed as

$$M_{i,T} = M_{i0} B_i(x_{i,T}) \quad (2)$$

$M_{i0}$  is the zero-temperature moment of the  $i$ -site =  $n J_i g_i \mu_B N_A$  (per mole) where  $n$  is the number of sites per formula unit = 2 for d-sites and 3 for a and c-sites,  $J_i$  is the total angular momentum and  $g_i$  is the Landé  $g$ -factor of the ion in the  $i$ -site,  $\mu_B$  is the Bohr magneton and  $N_A$  is Avogadro's number. The  $T$ -dependence is described by  $B_i$ , the Brillouin function for the sublattice, with argument  $x_{i,T}$ :

$$B_i(x_{i,T}) = \left[ \frac{2J_i + 1}{2J_i} \right] \coth \left[ \frac{2J_i + 1}{2J_i} x_{i,T} \right] - \left[ \frac{1}{2J_i} \right] \coth \left[ \frac{1}{2J_i} x_{i,T} \right]$$

where

$$x_{i,T} = \frac{J_i g_i \mu_B \mu_0}{kT} \sum_{j=a,d,c} N_{ij} M_{j,T}$$

(3)

$N_{ij}$  represents the molecular field coefficient (MFC) between the  $i$  and  $j$ -sites.

The MFCs  $N_{ij}$  quantify the exchange coupling both within a sublattice and between sublattices:  $N_{ij}$  is proportional to the exchange coupling  $J_{ij}$ . A negative sign of  $N_{ij}$  indicates parallel (ferromagnetic) coupling whereas positive indicates antiparallel coupling. Superexchange between the  $\text{Fe}^{3+}$  ions in the  $a$  and  $d$ -sites of iron garnets is described with a MFC of  $N_{ad} = 97 \text{ mol cm}^{-3}$  [19]. The intra-sublattice couplings within the  $a$  and  $d$ -sublattices are the next strongest, with  $N_{aa} = -65 \text{ mol cm}^{-3}$  and  $N_{dd} = -30.4 \text{ mol cm}^{-3}$  [19]. Coupling between  $\text{Fe}^{3+}$  and  $\text{RE}^{3+}$  is an order of magnitude smaller:  $N_{ac}$  and  $N_{cd}$  are shown in Table S1 for various  $c$ -site REs which came from fitting experimental data [25,31,65]. The coupling between REs in the  $c$ -sites is negligible, i.e.  $N_{cc}$  is taken as zero. The model does not account for spin reorientation or noncollinear magnetic order [41,42].

Although the molecular field coefficient model has been previously implemented for a range of bulk iron garnets [18–20,25,38,43–49], to our knowledge, MFC modeling has not been optimized for materials with non-ideal site occupancies such as antisite Fe or antisite RE. Furthermore, evaluating the Brillouin function is computationally demanding, requiring multiple sinusoidal functions, and each sublattice moment depends on the other sublattices, resulting in a system of non-linear equations. Our previous model [38] and Dionne's model written in Fortran [25] iteratively solved this system of equations by calculating the magnetization at each temperature from the sublattice moments at lower temperatures, creating inaccuracies at higher

temperatures. DIONNE recursively solves this system of equations at each temperature using `fsolve` in the `optimize` section of the SciPy Python library [50]. DIONNE is implemented in python to minimize both runtime and memory requirements for efficient processing. DIONNE is available on GitHub at <https://github.com/mjgross20/DIONNE>.

## Results and Discussion

### 1. REIGs with one or more rare earth element

We first model REIGs with one rare earth to validate the approach. Table S1 in the Supplementary Information [65] provides the angular momentum, Landé  $g$ -factor, and MFCs of each RE in the  $c$ -site, derived from theory and experimental fitting [20,25,31,35,51]. Figure 1a shows the resulting plots for several different REIGs, each with one rare earth, compared with the experimental results from Pauthenet [35]. Figure S1 shows additional examples plotted with past experimental and modeled results [25,28,30,31,35,52,65]. Inconsistencies between different experimentally reported results slightly alter the moment versus temperature curves, which can be accounted for with small modifications to the values in Table S1 [65]. The Curie temperature  $T_C$  is dominated by the coupling between the Fe on the  $a$ - and  $d$ -sites and is 560 K, independent of the RE, in agreement with experimental data [31,34,35]. A compensation temperature  $T_{\text{comp}}$  occurs for some REIGs where the net magnetic moment is zero.  $T_{\text{comp}} = 85$  K for ErIG, increasing to  $T_{\text{comp}} = 282$  K for GdIG in agreement with previously reported results [31,35,49]. Supplementary Note 1 [65] shows an excellent agreement of the model with experimental data.

In addition to the magnetization, DIONNE calculates the angular momentum as a function of temperature. This additional output is readily calculated from the magnetic moment and the Landé  $g$ -factors of each cation. Some REIG compositions yield an angular momentum compensation temperature,  $T_A$ , as shown in Figure 1b.  $T_A$  is important in determining the magnetization dynamics, for example the domain wall mobility in RE-transition metal alloys is maximum at  $T_A$  rather than at  $T_{\text{comp}}$  [53,54]. For GdIG,  $T_A = T_{\text{comp}} = 282$  K because all the cations,  $\text{Gd}^{3+}$  and  $\text{Fe}^{3+}$ , have the same  $g = 2$  [55]. In contrast,  $\text{Er}^{3+}$  has  $g = 1.38$  and ErIG has  $T_A = 130$  K, which is almost 50 K higher than its  $T_{\text{comp}}$ .

The properties of REIGs can be tuned by substitution of other REs on the c-sites. Coupling within the dodecahedral sublattice is negligible because there are no c-site nearest neighbors ( $N_{\text{cc}} = 0$ ). This allows us to model the c-site as an average of the occupying REs, following Dionne [25]. Figure 2 shows magnetization versus temperature of two different solid solutions, Gd-substituted YIG ( $\text{Gd}_x\text{Y}_{3-x}\text{Fe}_5\text{O}_{12}$ ), Fig. 2a, and Gd-substituted DyYIG ( $\text{Gd}_x\text{Dy}_{0.3}\text{Y}_{2.7-x}\text{Fe}_5\text{O}_{12}$ ), Fig. 2b. YIG has no compensation temperature, but adding Gd produces a  $T_{\text{comp}}$  for  $x > 0.6$  Gd per formula unit (f.u.) in  $\text{Gd}_x\text{Y}_{3-x}\text{Fe}_5\text{O}_{12}$  and  $x > \sim 0.3$  in  $\text{Gd}_x\text{Dy}_{0.3}\text{Y}_{2.7-x}\text{Fe}_5\text{O}_{12}$ . The calculated  $M(T)$  matches experimental data (see Supplementary Figure S2 [65]) [26,29,32].

Figure 3 compares the sublattice magnetization and angular momentum of  $\text{Dy}_1\text{Gd}_2\text{Fe}_5\text{O}_{12}$ , yielding  $T_{\text{comp}} = 267$  K and  $T_A = 296$  K. Fig. 3c evaluates  $T_{\text{comp}}$  and  $T_A$  of DyGdIG vs. composition for increasing amounts of Dy. The difference between the compensation temperatures ( $T_{\text{comp}} - T_A$ ) increases with Dy substitution as the average  $g$ -factor of the dodecahedral sites is reduced.

## 2. Point defects and non-bulk stoichiometry in rare earth iron garnets

Vacancies and non-magnetic substitutions have a large impact on the magnetic behavior of REIGs. Dionne [19] proposed that in YIG the zero-temperature magnetic moment and the MFCs of each Fe sublattice are affected by non-magnetic substitutions in both the Fe sublattices. Thus,  $M_{a0}$ ,  $M_{d0}$ ,  $N_{aa}$ ,  $N_{ad}$ , and  $N_{dd}$  become functions of the fraction of non-magnetic species (including vacancies) both in the a-site,  $k_a$ , and in the d-site,  $k_d$ , where  $0 \leq k_d, k_a < 1$ . Dionne's model included a linear scaling of  $M_{a0}$  with  $(1 - k_a)$  and  $M_{d0}$  with  $(1 - k_d)$  which fitted experimental data for  $0 \leq k_d < 0.65$ ,  $0 \leq k_a < 0.35$ , but at higher non-magnetic fractions the model diverged from experimental results. The deviation was attributed to canting of the magnetic moments of the non-substituted sublattice and was accounted for by including an empirical dependence of  $M_{a0}$  on  $(1 - k_d^{5.4})$  and  $M_{d0}$  on  $(1 - 0.1k_a)$  [19]. The fraction of non-magnetic species in the c-site,  $k_c$ , is included by linearly scaling  $M_{c0}$  with  $(1 - k_c)$  [25]. We adopted Dionne's expressions which are given in Supplementary Note 2 [19,65], modifying them to include antisite defects and divalent Fe as described in the remainder of this section.

Figs. 4a and b show magnetization versus temperature of YIG with increasing levels of octahedral and tetrahedral non-magnetic species, respectively. Non-magnetic species on either site dilute the superexchange between the Fe on the a and d sublattices by reducing the number of magnetic neighbors, and frustration of spins adjacent to the substituted site leads to spin canting and a reduction in the sublattice moment [21]. Nonmagnetic substitutions therefore reduce  $T_C$  and the values of the MFCs. However, octahedral and tetrahedral non-magnetic species have opposing effects on the low temperature net magnetization  $M_0$ : increasing  $k_a$  raises  $M_0$  by reducing the moment of the minority sublattice, whereas increasing  $k_d$  lowers  $M_0$ . Figure 4c shows the special case of antiferromagnetic YIG where 1/3 of the tetrahedral Fe is replaced by a

trivalent nonmagnetic substituent, yielding a Néel temperature of 440K. Figure 5a,b shows the agreement of DIONNE with experimental data [56].

The Fe in REIGs is trivalent, but oxygen deficiency or tetravalent cations promote the formation of  $\text{Fe}^{2+}$  for charge balance [57,58]. As a larger ion than  $\text{Fe}^{3+}$ , the  $\text{Fe}^{2+}$  preferentially occupies the octahedral sites. DIONNE can account for a-site  $\text{Fe}^{2+}$  ( $4 \mu_B$ ) replacing  $\text{Fe}^{3+}$  ( $5 \mu_B$ ) by adjusting the zero-temperature magnetic moment of the a-site sublattice  $M_{a0}$  (see Supplementary Note 2 [65]) while using the same MFC values for  $\text{Fe}^{2+}$  that were used for  $\text{Fe}^{3+}$ . Fig. 5c shows  $M(T)$  for increasing levels of  $\text{Fe}^{2+}$  in YIG.  $T_C$  decreases as  $\text{Fe}^{2+}$  increases because  $\text{Fe}^{2+}$  lowers the octahedral sublattice moment  $M_{a0}$  and hence the inter-sublattice coupling, Eq. 3. Previous studies of YIG and substituted YIG containing  $\text{Fe}^{2+}$  find a decrease in  $T_C$  [57,58].

Bulk REIGs exhibit little variation from the ideal RE:Fe = 0.6 stoichiometry [59–61]. However, thin films of REIGs with compositions that deviate substantially from the ideal RE:Fe ratio can be stabilized by epitaxial growth on a garnet substrate [36]. To model these antisite defects, we consider the effects of  $\text{Fe}^{3+}$  in the c-site for Fe-rich REIGs and  $\text{RE}^{3+}$  in the a-sites for RE-rich REIGs. We consider excess RE to occupy the a-sites and not the d-sites on steric grounds. DIONNE then needs to account for modifications in the zero-temperature moments of each sublattice, the inter- and intra-sublattice MFCs, and the Brillouin functions that describe the moment of each species and sublattice.

The zero-temperature moments are taken as functions of RE in the a-sites,  $k_{aR}$ , and Fe in the c-sites,  $k_{cF}$ . The relationships are based on those developed in [19] for non-magnetic substitutions  $k_a$ ,  $k_d$ , and  $k_c$ . We assume that intra-sublattice coupling is weak between the RE ions

in the a-sites due to their low concentration, and similarly that coupling is weak between Fe ions in the c-sites, enabling an analogous treatment to that of multiple RE ions in the c-sites [25]. First, we create additional sublattice terms to model the antisite magnetic ions with unique MFCs. For excess RE we modify the zero-T moment of the a-sites by reducing the a-site Fe contribution by  $k_{aR}$ . We add back the RE contribution via a new term,  $M_{aR0}$ , which includes the J and g-factor of the RE (see Table S1 [65]). In the case of excess Fe, we reduce the c-site RE contribution by  $k_{cF}$  and add back the Fe contribution via a new term,  $M_{cF0}$ . The general model then includes the following terms:

$$M_{d0} = 3\mu_B N_A S_F g_F (1 - k_d) (1 - 0.1(k_a + k_{aR})) \quad (4)$$

$$M_{a0} = 2\mu_B N_A [(1 - k_{F2})S_F + k_{F2}S_{F2}] g_F (1 - k_a - k_{aR}) (1 - k_d^{5.4}) \quad (5)$$

$$M_{aR0} = 2\mu_B N_A J'_R g_R k_{aR} (1 - k_d^{5.4}) \quad (6)$$

$$M_{c0} = 3\mu_B N_A J'_R g_R (1 - k_c - k_{cF}) \quad (7)$$

$$M_{cF0} = 3\mu_B N_A S_F g_F k_{cF} \quad (8)$$

where g is the Landé g-factor of the respective element,  $J'_R$  is the effective angular momentum of the RE element (introduced to account for canting of the RE at low temperatures due to magnetocrystalline anisotropy [25]), and  $S_F$  and  $S_{F2}$  are the spin angular momenta of  $\text{Fe}^{3+}$  and  $\text{Fe}^{2+} = 5/2$  and 2 respectively.

Second, we modify the formulae for  $N_{dd}$ ,  $N_{aa}$ , and  $N_{ad}$  to include the effects of  $k_{aR}$  and  $k_{cF}$  (see Supplementary Note 3 [65]), analogous to the effects of  $k_a$  and  $k_c$  [19].  $N_{ac}$  and  $N_{cd}$  are over an order of magnitude smaller; thus, the effects of  $k_{aR}$  and  $k_{cF}$  on them are neglected. We also introduce additional MFCs for the antisite cations. For  $RE^{3+}$  occupying octahedral sites,  $N_{aaR}$  and  $N_{aRd}$  describe the couplings between the a-site  $RE^{3+}$  with the a-site  $Fe^{3+}$  and d-site  $Fe^{3+}$  respectively.  $N_{acF}$  and  $N_{cFd}$  quantify the couplings between c-site  $Fe^{3+}$  with the a and d-site  $Fe^{3+}$  respectively. We neglect coupling between c-site Fe and octahedral RE ions following similar reasoning for neglecting  $N_{cc}$  (see Supplementary Note 4 [65]). Initial guesses for the MFCs are based on the MFCs of the ions in their usual sites, and then further adjusted by comparison with experimental data. For example,  $Tb^{3+}$  in the dodecahedral sublattice has  $N_{ac}$  and  $N_{cd}$  of -4.2 and 6.5 mol cm<sup>-3</sup> respectively for stoichiometric TbIG. To model Tb-rich TbIG, we initially set  $N_{aaR}$  and  $N_{aRd}$  to -4.2 and 6.5 respectively. These values are then fine-tuned to match experimental results as shown below.

We illustrate the application of DIONNE by fitting  $M(T)$  data for a Tb-rich TbIG film reported by Rosenberg, et al. [38] with  $T_{comp} = 330 \pm 10$  K (higher than that of bulk TbIG, 250 K) and  $T_C = 490 \pm 10$  K. X-ray photoelectron spectroscopy, transmission electron microscopy, and X-ray magnetic circular dichroism confirmed the presence of excess Tb in the octahedral sites, with  $Tb:Fe = 0.86$ ,  $Fe_{oct}:Fe_{tet} = 0.602$ , and negligible  $Fe^{2+}$ . The  $Fe_{oct}:Fe_{tet}$  ratio implies the presence of vacancies on at least the tetrahedral sites because the excess Tb occupies the octahedral sites. Our previous iterative MFC model [38] was used to determine the site occupancies by fitting only to the measured  $T_{comp}$ , yielding a stoichiometry of  $\{Tb_3^{3+}\}[Fe_{1.35}V_{0.55}Tb_{0.097}^{3+}](Fe_{2.25}V_{0.75})O_{12-\delta}^{-2}$  where {}, [], and () are the c, a and d-sites respectively. This stoichiometry indicates substantial

concentrations of vacancies and oxygen deficiency,  $\delta = 1.95$  [38], which are larger than has been reported experimentally [62].

Using DIONNE, we obtained an excellent fit to  $T_{\text{comp}}$ ,  $T_C$ , and the magnetic moment of the experimental data for a composition of  $\{Tb_3^{3+}\}[Fe_{1.52}Tb_{0.48}](Fe_{2.53}^{3+}V_{0.47})O_{12-\delta}^{-2}$  as shown in Figure 6a,b. We arrived at this stoichiometry by first considering combinations of  $k_a$ ,  $k_d$ , and  $k_{aR}$  that are consistent with the experimental data. DIONNE gave the best agreement to the experimental value of  $T_C$  when Fe vacancies were minimized. Since vacancies need only be present on the d-sites, we take  $k_a = 0$ , which implies  $k_d = 0.47/3 = 0.16$  and  $k_{aR} = 0.48/2 = 0.24$ . Next,  $T_{\text{comp}}$  was fit to the experimental data by varying the MFCs of the a-site  $Tb^{3+}$ , which had initially been set to the values for the c-site occupancy:  $N_{ac} = -4.2$  and  $N_{cd} = 6.2 \text{ mol cm}^{-3}$ . The best fit was obtained for  $N_{aR} = -2.8$  and  $N_{aRd} = 8.3 \text{ mol cm}^{-3}$ . Lastly,  $M(T)$  was calculated from the selected stoichiometry for the Tb-rich film which produced a good fit to the experimental data, Figure 6. Table I shows the fit parameters for the model of the Tb-rich film and for bulk TbIG. DIONNE's best fit yields a lower vacancy concentration than the model in [38], implying a lower oxygen deficiency,  $\delta = 0.31$  versus 1.95, for charge balance, which is and in better agreement with other reports [62,63]. In addition, DIONNE fits  $T_C$  as well as  $T_{\text{comp}}$ , showing a better high-temperature performance compared to the iterative model in [38].

A complementary case is presented by Fe-rich TbIG reported in [64]. Excess Fe led to a decrease in  $T_{\text{comp}}$ , opposite to the case of Tb-rich TbIG. To model the c-site Fe, we estimate  $N_{acF}$  and  $N_{cFd}$  to be -6.5 and 9.7  $\text{mol cm}^{-3}$  respectively, approximately an order a magnitude smaller than  $N_{aa}$  and  $N_{ad}$ . DIONNE reproduces the experimental trend, showing  $T_{\text{comp}}$  decreasing as a function of the Tb:Fe ratio, Fig. 6c.  $T_C$  was not reported in [64]; however, Fig. 6c shows  $T_C$  depends little

on the Tb:Fe ratio. Instead, Fe<sup>3+</sup> vacancies and substitutions have a significant effect on both  $T_C$  and  $T_{\text{comp}}$ .

## **Conclusion**

In summary, we developed DIONNE, a python computer program that uses molecular field coefficients to model the magnetic behavior of REIGs. The program calculates both the magnetization and angular momentum of each sublattice as functions of temperature for a REIG, yielding the compensation temperatures  $T_A$  and  $T_{\text{comp}}$  and the Curie temperature,  $T_C$ . DIONNE can also account for a wider range of point defects, substitutions, and stoichiometries than previously reported models [18–20,25,38,43–48] by considering the effects on the zero-temperature magnetization and sublattice coupling. Deviations from the RE:Fe = 3:5 stoichiometry were captured by introducing an additional sublattice moment to account for the excess Fe or RE in addition to modifying the relevant zero-temperature moments and MFCs. Comparison with experimental data from a Tb-rich TbIG film [38] enabled the site occupancy to be fitted to give a good quantitative agreement to the measured  $T_{\text{comp}}$  and  $T_C$  and implying the existence of tetrahedral vacancies. This modeling approach will facilitate the design of ferrimagnets with useful magnetic and spintronic properties.

## **Acknowledgements**

The authors would like to acknowledge support from the National Science Foundation under award DMR2152528.

## References

- [1] Y. Zhang, X. Feng, Z. Zheng, Z. Zhang, K. Lin, X. Sun, G. Wang, J. Wang, J. Wei, P. Vallobra, et al., *Ferrimagnets for Spintronic Devices: From Materials to Applications*, *Appl Phys Rev* **10**, 011301 (2023).
- [2] S. K. Kim, G. S. D. Beach, K. J. Lee, T. Ono, T. Rasing, and H. Yang, *Ferrimagnetic Spintronics*, *Nat Mater* **21**, 24 (2022).
- [3] Y. Kajiwara, K. Harii, S. Takahashi, J. Ohe, K. Uchida, M. Mizuguchi, H. Umezawa, H. Kawai, K. Ando, K. Takanashi, et al., *Transmission of Electrical Signals by Spin-Wave Interconversion in a Magnetic Insulator*, *Nature* **464**, 262 (2010).
- [4] J. A. González, J. P. Andrés, and R. L. Antón, *Applied Trends in Magnetic Rare Earth/Transition Metal Alloys and Multilayers*, *Sensors* **21**, 5615 (2021).
- [5] K. Srinivasan and B. J. H. Stadler, *Review of Integrated Magneto-Optical Isolators with Rare-Earth Iron Garnets for Polarization Diverse and Magnet-Free Isolation in Silicon Photonics [Invited]*, *Opt Mater Express* **12**, 697 (2022).
- [6] J. F. Barry, R. A. Irion, M. H. Steinecker, D. K. Freeman, J. J. Kedziora, R. G. Wilcox, and D. A. Braje, *Ferrimagnetic Oscillator Magnetometer*, *Phys Rev Appl* **19**, 044044 (2023).
- [7] H. Chang, P. Li, W. Zhang, T. Liu, A. Hoffmann, L. Deng, and M. Wu, *Nanometer-Thick Yttrium Iron Garnet Films with Extremely Low Damping*, *IEEE Magn Lett* **5**, 1 (2014).
- [8] O. Ciubotariu, A. Semisalova, K. Lenz, and M. Albrecht, *Strain-Induced Perpendicular Magnetic Anisotropy and Gilbert Damping of Tm<sub>3</sub>Fe<sub>5</sub>O<sub>12</sub> Thin Films*, *Sci Rep* **9**, 17474 (2019).
- [9] Y. Zhao, Y. Li, S. Zhu, C. Chen, M. Yao, Y. Zhao, Z. Hu, B. Peng, M. Liu, and Z. Zhou, *Voltage Tunable Low Damping YIG/PMN-PT Multiferroic Heterostructure for Low-Power RF/Microwave Devices*, *J Phys D Appl Phys* **54**, 245002 (2021).
- [10] C. Hauser, T. Richter, N. Homonnay, C. Eisenschmidt, M. Qaid, H. Deniz, D. Hesse, M. Sawicki, S. G. Ebbinghaus, and G. Schmidt, *Yttrium Iron Garnet Thin Films with Very Low Damping Obtained by Recrystallization of Amorphous Material*, *Sci Rep* **6**, 20827 (2016).
- [11] C. O. Avci, E. Rosenberg, M. Baumgartner, L. Beran, A. Quindeau, P. Gambardella, C. A. Ross, and G. S. D. Beach, *Fast Switching and Signature of Efficient Domain Wall Motion Driven by Spin-Orbit Torques in a Perpendicular Anisotropy Magnetic Insulator/Pt Bilayer*, *Appl Phys Lett* **111**, 072406 (2017).
- [12] S. Vélez, J. Schaab, M. S. Wörnle, M. Müller, E. Gradauskaite, P. Welter, C. Gutgsell, C. Nistor, C. L. Degen, M. Trassin, et al., *High-Speed Domain Wall Racetracks in a Magnetic Insulator*, *Nat Commun* **10**, 4750 (2019).
- [13] L. J. Cornelissen, J. Liu, R. A. Duine, J. Ben Youssef, and B. J. Van Wees, *Long-Distance Transport of Magnon Spin Information in a Magnetic Insulator at Room Temperature*, *Nat Phys* **11**, 1022 (2015).

- [14] L. Soumah, N. Beaulieu, L. Qassym, C. Carrétéro, E. Jacquet, R. Lebourgeois, J. Ben Youssef, P. Bortolotti, V. Cros, and A. Anane, *Ultra-Low Damping Insulating Magnetic Thin Films Get Perpendicular*, *Nat Commun* **9**, 3355 (2018).
- [15] A. Quindeau, C. O. Avci, W. Liu, C. Sun, M. Mann, A. S. Tang, M. C. Onbasli, D. Bono, P. M. Voyles, Y. Xu, et al., *Tm<sub>3</sub>Fe<sub>5</sub>O<sub>12</sub>/Pt Heterostructures with Perpendicular Magnetic Anisotropy for Spintronic Applications*, *Adv Electron Mater* **3**, 1600376 (2017).
- [16] J. J. Bauer, E. R. Rosenberg, S. Kundu, K. A. Mkhoyan, P. Quarterman, A. J. Grutter, B. J. Kirby, J. A. Borchers, and C. A. Ross, *Dysprosium Iron Garnet Thin Films with Perpendicular Magnetic Anisotropy on Silicon*, *Adv Electron Mater* **6**, 1900820 (2020).
- [17] M. L. Néel, *Propriétés Magnétiques Des Ferrites; Ferrimagnétisme et Antiferromagnétisme*, *Ann Phys (Paris)* **12**, 137 (1948).
- [18] A. E. Clark and E. Callen, *Néel Ferrimagnets in Large Magnetic Fields*, *J Appl Phys* **39**, 5972 (1968).
- [19] G. F. Dionne, *Molecular Field Coefficients of Substituted Yttrium Iron Garnets*, *J Appl Phys* **41**, 4874 (1970).
- [20] C. D. Brandle and S. L. Blank, *Magnetic Moments for Mixed Substituted Rare Earth Iron Garnets*, *IEEE Trans Magn* **12**, 14 (1976).
- [21] G. F. Dionne, *Origin of Exchange Field Reductions in Diluted Magnetic Garnets*, *J Appl Phys* **85**, 4627 (1999).
- [22] G. F. Dionne and P. F. Tumelty, *Molecular-Field Coefficients of Tm<sub>3</sub>Fe<sub>5</sub>O<sub>12</sub>*, *J Appl Phys* **50**, 8257 (1979).
- [23] G. F. Dionne, *Molecular-Field Coefficients of Rare-Earth Iron Garnets*, *J Appl Phys* **47**, 4220 (1976).
- [24] G. F. Dionne, *Molecular Field and Exchange Constants of Gd<sup>3+</sup>- Substituted Ferrimagnetic Garnets*, *J Appl Phys* **42**, 2142 (1971).
- [25] G. F. Dionne, *Magnetic Moment Versus Temperature Curves of Rare-Earth Iron Garnets*, MIT Lincoln Laboratory Technical Report (1979).
- [26] E. E. Anderson, J. R. Cunningham, and G. E. McDuffie, *Magnetic Properties of the Mixed Garnets (3-x)Y<sub>2</sub>O<sub>3</sub>•xGd<sub>2</sub>O<sub>3</sub>•5Fe<sub>2</sub>O<sub>3</sub>*, *Physical Review* **116**, 624 (1959).
- [27] G. Villers, J. Lories, and C. Claudel, *Magnétisme - Quelques Propriétés Des Grenats Mixtes de Gadolinium-Erbium et de Gadolinium-Yttrium*, *C. R. Acad. Sci.* **247**, 710 (1958).
- [28] A. Vassiliev, J. Nicolas, and M. Hildebrandt, *Magnétisme - Sur Les Propriétés Des Grenats Mixtes d'yttrium-Holmium*, *C. R. Acad. Sci.* **253**, 242 (1961).
- [29] A. Vassiliev, J. Nicolas, and M. Hildebrandt, *Magnétisme - Sur Les Propriétés Des Grenats Mixtes d'yttrium-Gadolinium*, *C. R. Acad. Sci.* **252**, 2529 (1961).
- [30] A. Vassiliev, J. Nicolas, and M. Hildebrandt, *Magnétisme - Sur Les Propriétés Des Grenats Mixtes d'yttrium-Dysprosium*, *C. R. Acad. Sci.* **252**, 2681 (1961).
- [31] S. Geller, J. P. Remeika, R. C. Sherwood, H. J. Williams, and G. P. Espinosa, *Magnetic Study of the Heavier Rare-Earth Iron Garnets*, *Physical Review* **137**, A1034 (1965).
- [32] G. R. Harrison and L. R. Hodges, *Temperature Stable Microwave Hybrid Garnets*, *J Appl Phys* **33**, 1375 (1962).

- [33] R. Pauthenet, *Spontaneous Magnetization of Some Garnet Ferrites and the Aluminum Substituted Garnet Ferrites*, J Appl Phys **29**, 253 (1958).
- [34] R. Pauthenet, *Magnetic Properties of the Rare Earth Garnets*, J Appl Phys **30**, S290 (1959).
- [35] R. Pauthenet, *Les Propriétés Magnétiques Des Ferrites d'yttrium et de Terres Rares de Formule  $5Fe_2O_3 \cdot 3M_2O_3$* , Ann Phys (Paris) **13**, (1958).
- [36] T. Su, S. Ning, E. Cho, and C. A. Ross, *Magnetism and Site Occupancy in Epitaxial Y-Rich Yttrium Iron Garnet Films*, Phys Rev Mater **5**, 094403 (2021).
- [37] G. F. Dionne, *Magnetic Oxides* (Springer US, 2009).
- [38] E. Rosenberg, J. Bauer, E. Cho, A. Kumar, J. Pellicciari, C. A. Occhialini, S. Ning, A. Kaczmarek, R. Rosenberg, J. W. Freeland, et al., *Revealing Site Occupancy in a Complex Oxide: Terbium Iron Garnet*, Small **19**, 2300824 (2023).
- [39] G. F. Dionne, *Molecular-Field Coefficients of  $MnFe_2O_4$  and  $NiFe_2O_4$  Spinel Ferrite Systems*, J Appl Phys **63**, 3777 (1988).
- [40] G. F. Dionne, *High Magnetization Limits of Spinel Ferrite*, J Appl Phys **61**, 3865 (1987).
- [41] B. Tomasello, D. Mannix, S. Geprägs, and T. Ziman, *Origin and Dynamics of Umbrella States in Rare-Earth Iron Garnets*, Ann Phys (N Y) **447**, (2022).
- [42] A. Boutaba, M. Lahoubi, V. Varazashvili, and S. Pu, *Magnetic, Magneto-Optical and Specific Heat Studies of the Low Temperature Anomalies in the Magnetodielectric  $DyIG$  Ferrite Garnet*, Journal of Magnetism and Magnetic Materials.
- [43] J. Cieslak, M. Reissner, J. Dabrowa, and K. Zielinska, *Magnetization Measurements of Multicomponent Iron Garnets*, J Magn Magn Mater **582**, 170987 (2023).
- [44] V. Joch, P. Molho, and L. Ranno, *Magnetization Processes in a Dot of Ferrimagnetic Garnet near the Compensation Temperature*, J Phys Conf Ser **303**, 012006 (2011).
- [45] J. Bernasconi and D. Kuse, *Canted Spin Phase in Gadolinium Iron Garnet*, Phys Rev B **3**, 811 (1971).
- [46] E. E. Anderson, *Molecular Field Model and the Magnetization of YIG*, Physical Review **134**, A1581 (1964).
- [47] R. Z. Levitin, B. K. Ponomarev, and Y. F. Popov, *Magnetization of Iron Garnets of Heavy Rare Earth Elements in Fields up to 240 KOe*, Soviet Physics JETP **59**, 1952 (1971).
- [48] W. Wang, R. Chen, and X. Qi, *Analysis on Three-Sublattice Model of Magnetic Properties in Rare-Earth Iron Garnets under High Magnetic Fields*, J Alloys Compd **512**, 128 (2012).
- [49] A. Budkowski, A. Szytuła, D. Rodic, R. Duraj, J. Mayer, J. Sciesinski, and V. Spasojevic, *The Compensation Point in Reig and Some of Its Properties*, J Magn Magn Mater **78**, 226 (1989).
- [50] P. Virtanen, R. Gommers, T. E. Oliphant, M. Haberland, T. Reddy, D. Cournapeau, E. Burovski, P. Peterson, W. Weckesser, J. Bright, et al., *SciPy 1.0: Fundamental Algorithms for Scientific Computing in Python*, Nat Methods **17**, 261 (2020).
- [51] R. Aléonard, *Etude Paramagnetique Des Ferrites D'yttrium et de Terres Rares de Formule  $5Fe_2O_3 \cdot 3M_2O_3$* , Journal of Physics and Chemistry of Solids **15**, 167 (1960).

- [52] W. P. Wolf and J. H. Van Vleck, *Magnetism of Europium Garnet*, Physical Review **118**, (1960).
- [53] M. Binder, A. Weber, O. Mosendz, G. Woltersdorf, M. Izquierdo, I. Neudecker, J. R. Dahn, T. D. Hatchard, J. U. Thiele, C. H. Back, et al., *Magnetization Dynamics of the Ferrimagnet CoGd near the Compensation of Magnetization and Angular Momentum*, Phys Rev B Condens Matter Mater Phys **74**, 134404 (2006).
- [54] S. A. Siddiqui, J. Han, J. T. Finley, C. A. Ross, and L. Liu, *Current-Induced Domain Wall Motion in a Compensated Ferrimagnet*, Phys Rev Lett **121**, 057701 (2018).
- [55] B. A. Calhoun, W. V. Smith, and J. Overmeyer, *Ferrimagnetic Resonance in Gadolinium Iron Garnet*, J Appl Phys **29**, 427 (1958).
- [56] M. A. Gilleo and S. Geller, *Magnetic and Crystallographic Properties of Substituted Yttrium-Iron Garnet,  $3Y_2O_3 \cdot xM_2O_3 \cdot (5-x)Fe_2O_3$* , Physical Review **110**, 73 (1958).
- [57] E. Baños-López, C. A. Cortés-Escobedo, F. Sánchez-De Jesús, A. Barba-Pingarrón, and A. M. Bolarín-Miró, *Crystal Structure and Magnetic Properties of Cerium-Doped YIG: Effect of Doping Concentration and Annealing Temperature*, J Alloys Compd **730**, 127 (2018).
- [58] V. Sharma and B. K. Kuanr, *Magnetic and Crystallographic Properties of Rare-Earth Substituted Yttrium-Iron Garnet*, J Alloys Compd **748**, 591 (2018).
- [59] G. P. Espinosa, *Crystal Chemical Study of the Rare-Earth Iron Garnets*, J Chem Phys **37**, 2344 (1962).
- [60] W. A. Bonner, *A Novel Non-Pb Flux System for the Preparation of Yttrium and Rare Earth Iron Gallium and Aluminum Garnets*, Mater Res Bull **12**, 289 (1977).
- [61] A. Paoletti, *Physics of Magnetic Garnets* (North-Holland Pub. Co., Amsterdam, 1979).
- [62] S. A. Manuilov, S. I. Khartsev, and A. M. Grishin, *Pulsed Laser Deposited  $Y_3Fe_5O_{12}$  Films: Nature of Magnetic Anisotropy  $i$* , J Appl Phys **106**, 123917 (2009).
- [63] Y. Dumont, N. Keller, E. Popova, D. S. Schmool, S. Bhattacharya, B. Stahl, M. Tessier, and M. Guyot, *Superexchange and Iron Valence Control by Off-Stoichiometry in Yttrium Iron Garnet Thin Films Grown by Pulsed Laser Deposition*, J Appl Phys **97**, 10G108 (2005).
- [64] S. Damerio and C. O. Avci, *Sputtered Terbium Iron Garnet Films with Perpendicular Magnetic Anisotropy for Spintronic Applications*, J Appl Phys **133**, 073902 (2023).
- [65] See Supplemental Material at [url] for additional examples of DIONNE and details of the formulas used in the model.

## Tables and Figures

**Table I.** Fit parameters for Tb-rich TbIG in Figure 6 compared to bulk TbIG.

	Bulk TbIG	Tb-rich TbIG
$k_a$ (fraction of vacancies on a-site)	0	0

$k_d$  (fraction of vacancies on d-site)  
 $k_{aR}$  (fraction of Tb on a-site)  
 $N_{ad}$  (coupling of a-site with d-site Fe)  
 $N_{aa}$  (coupling of a-site with a-site Fe)  
 $N_{dd}$  (coupling of d-site with d-site Fe)  
 $N_{cd}$  (coupling of c-site Tb with d-site Fe)  
 $N_{ca}$  (coupling of c-site Tb with a-site Fe)  
 $N_{aaR}$  (coupling of a-site Fe with a-site Tb)  
 $N_{aRd}$  (coupling of a-site Tb with d-site Fe)

0	0.16
0	0.24
97 mol cm <sup>-3</sup>	91.21 mol cm <sup>-3</sup>
-65 mol cm <sup>-3</sup>	-52.17 mol cm <sup>-3</sup>
-30.4 mol cm <sup>-3</sup>	-22.37 mol cm <sup>-3</sup>
6.5 mol cm <sup>-3</sup>	6.50 mol cm <sup>-3</sup>
-4.2 mol cm <sup>-3</sup>	-4.20 mol cm <sup>-3</sup>
--	-2.80 mol cm <sup>-3</sup>
--	8.30 mol cm <sup>-3</sup>

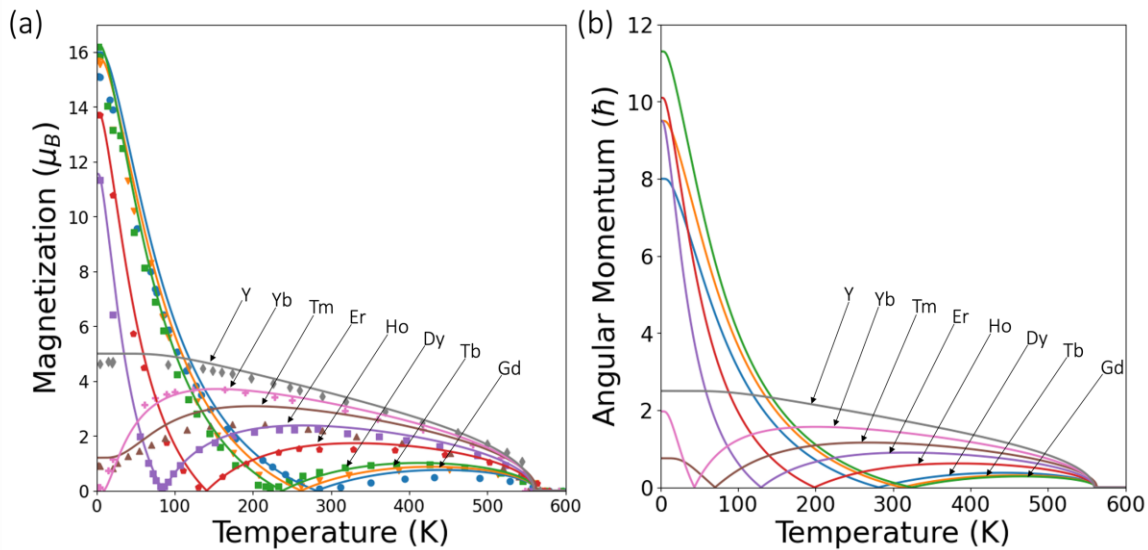


**Figure 1.** Magnetic moment (a) and angular momentum (b) versus temperature curves of 8 different REIGs, with each curve color corresponding to the indicated RE. In (a), lines are from our model and data points from Pauthenet [35]. Further comparisons with both experimental data [25,28,30,35,52] and Dionne's model [25] are shown in Figure S1 [65]. Magnetization is plotted in  $\mu_B$ /formula unit (f.u.), angular momentum is in units of  $\hbar/2\pi$  per formula unit.

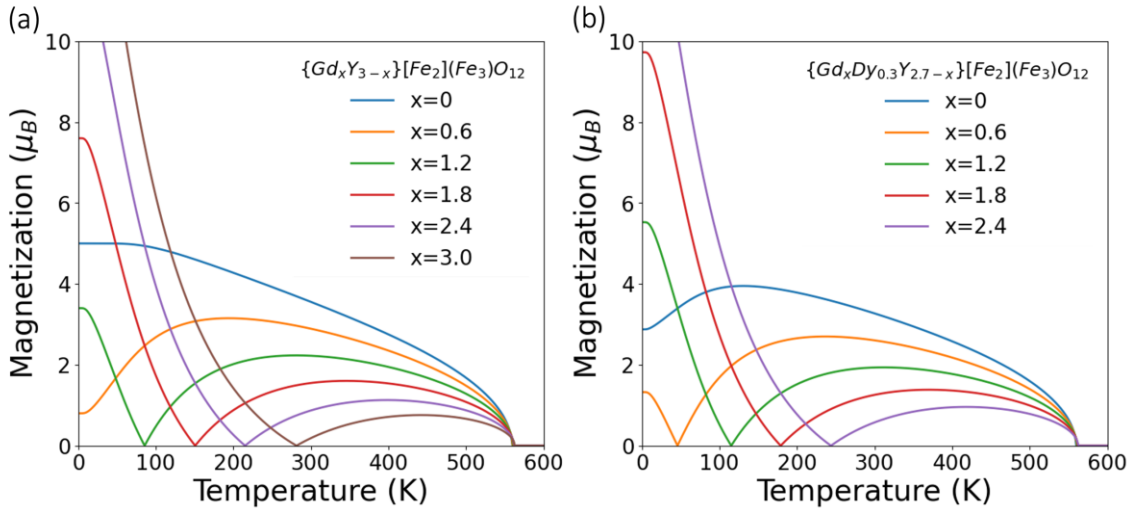


**Figure 2.** Magnetization versus temperature curves of REIGs GdYIG (a) and GdDyYIG (b).  $x$  represents the amount of Gd substituted into (a) YIG and (b) DyYIG with 0.3 Dy/f.u.

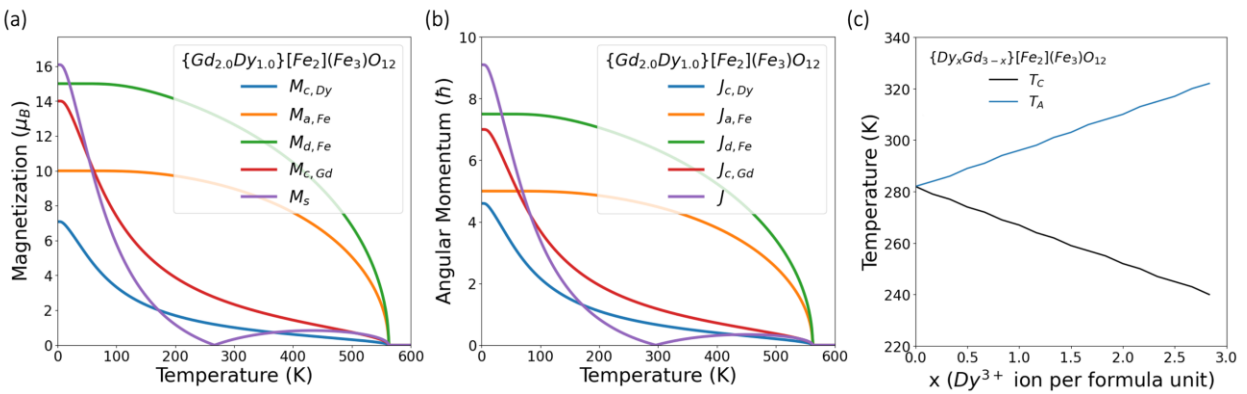


**Figure 3.** Magnetic modeling of DyGdIG. (a) Magnetization and (b) angular momentum vs. temperature curve of  $Dy_1Gd_2Fe_5O_{12}$  for the individual sublattices and the total per f.u. (c) Magnetic compensation and angular momentum compensation vs. composition.

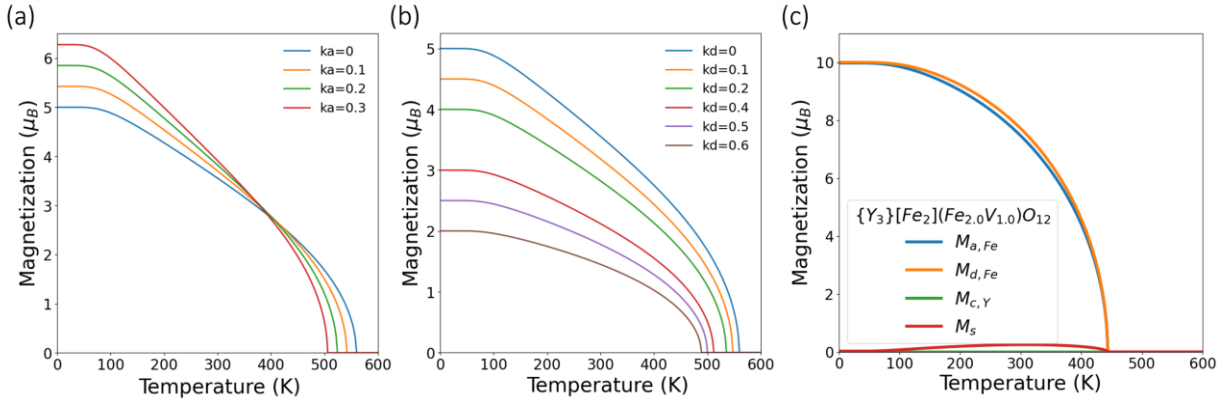


**Figure 4.** Magnetization versus temperature curves for (a) octahedral and (b) tetrahedral vacancies or non-magnetic substitutions in YIG. (c) Antiferromagnetic YIG is simulated by substituting 1/3 of the tetrahedral Fe with a non-magnetic species or vacancy V, assumed trivalent for charge balance. Since the coupling in the d-sites and a-sites differs, there is a small net moment between 150 K and 450 K.

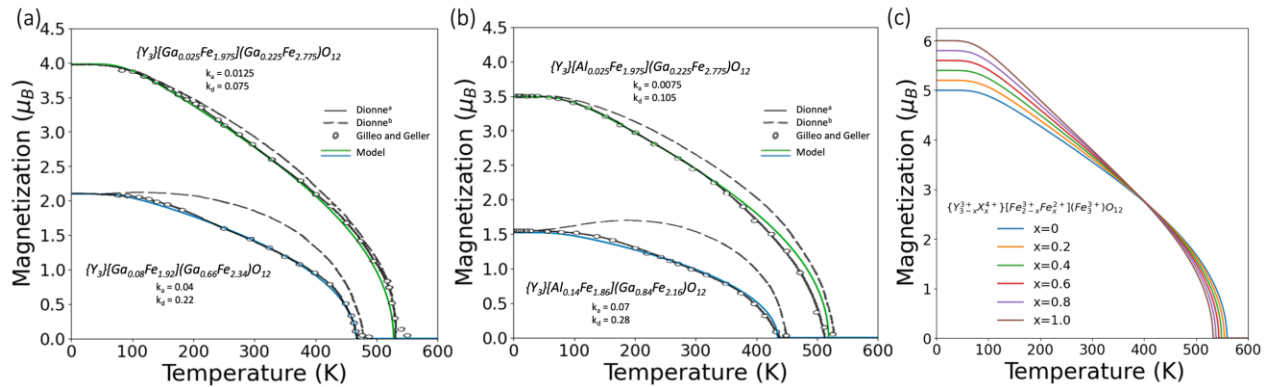


**Figure 5.** Magnetization vs. temperature curves of YIG with several Fe substitutions. (a) Ga and (b) Al-substituted YIG are plotted with the corresponding a- and d-site substitutions  $k_d$  and  $k_a$ . Model data is shown in color, compared with experimental data [56] and calculated data from Dionne [19] with (a, solid line) and without (b, dashed line) modifying the MFCs of Fe due to the

non-magnetic substitutions. (c)  $\text{Fe}^{2+}$  in octahedral sites in YIG, where X represents a nonmagnetic tetravalent ion for charge balance.

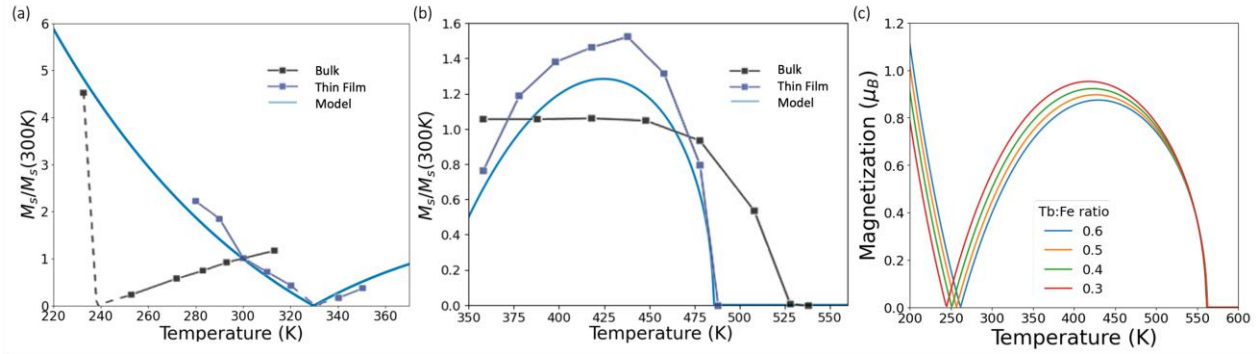


**Figure 6.** Magnetization versus temperature curves of Tb-rich TbIG data reported from Rosenberg, et al. [38] and DIONNE fitting the data near (a) the compensation temperature and (b) the Curie temperature. Magnetization is normalized by the moment at 300 K. (c) Magnetization versus temperature curves of Fe-rich TbIG, where excess Fe is present on the c-sites and there are no vacancies included.